Fermilab Library
0 1160 0038669 2

330

MIDWESTERN UNIVERSITIES RESEARCH ASSOCIATION

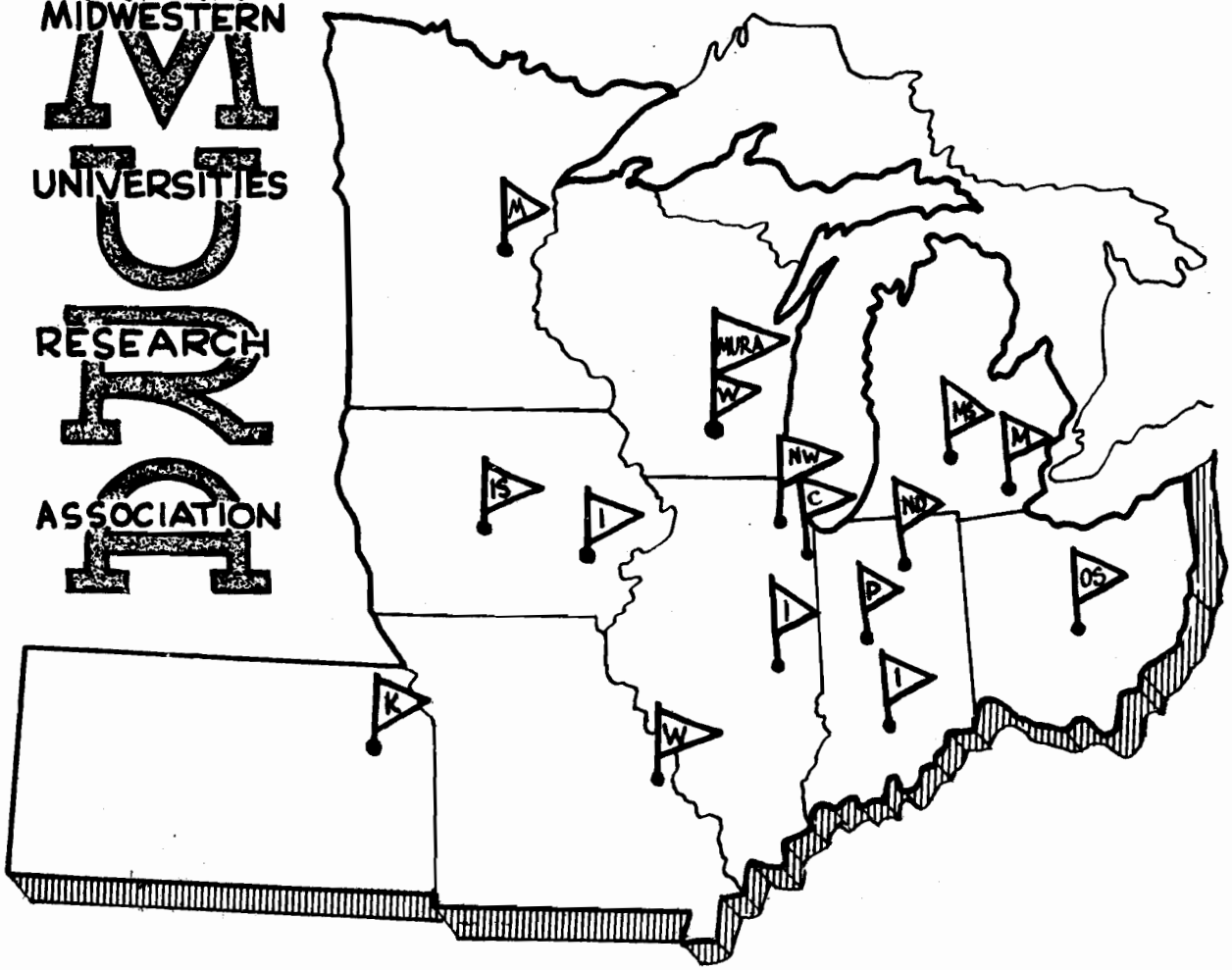

Beam Stacking Experiments In An Electron Model FFAG Accelerator

August 1, 1957

(Submitted to the Review of Scientific Instruments)

REPORT **NUMBER** 330

Beam Stacking Experiments In An Electron Model FFAG Accelerator*

K.M. Terwilliger**, L.W. Jones** and C.H. Pruett

Midwestern Universities Research Association

Madison, Wisconsin

ABSTRACT

A number of experiments are described which test the interactions of particles with rf accelerating voltages in an FFAG accelerator. The experiments confirm predictions of a theory of Symon and Sessler and demonstrate the feasibility of "stacking" successively accelerated groups of particles with a density close to that of a single group.

* Supported by the U.S. Atomic Energy Commission

** On leave from the University of Michigan, Ann Arbor, Michigan

I. INTRODUCTION

The use of intersecting beams as a means of producing very high center-of-mass energies has been re-proposed recently[1]. This proposal is based on the FFAG type of accelerator[2] which makes the required intensities appear feasible. The central point in such a scheme is the possibility of stacking a large number of pulses of rf accelerated particles into a small energy and radius interval so that the continuous intersection of two such circulating beams will produce a reasonable interaction rate. Beam stacking has been experimentally demonstrated by Crawford and Stubbins[3], who have stored up to seven pulses in the Berkeley 184 in. cyclotron. Symon and Sessler have developed a theory for rf acceleration[4] which predicts particle behavior in such a stacking process and gives the maximum number of pulses that can be stacked in a given energy interval. With their results the particle densities that appear attainable are sufficient for practical colliding beam experiments.

The FFAG electron model accelerator described in a previous paper[5] has been used to study beam stacking and in particular to check some of the predictions of the rf theory. The present paper describes these investigations and their results. The rf theory and its application to beam stacking are reviewed in Sec. II. Sec. III covers the experimental techniques and measurements. Sec. IV presents two experiments on ordinary rf acceleration and compares the results with expected values. Sec. V describes the experiments on beam stacking. These include quantitative measurements of the behavior of non-synchronous particles and a demonstration of the mechanism of beam stacking. The results are compared with

theoretical predictions. Conclusions are summarized in Sec. VI.

II. THEORY

The theory of radio frequency acceleration in synchrotrons using pulsed guide fields is well established[6] and carries over to accelerators using fixed guide fields without major modification[2]. However in the past these theories have not been concerned with particles out of synchronism with the accelerating rf. More recently Symon and Sessler[4] have treated the general rf problem by introducing canonical variables which may be used to construct a Hamiltonian, allowing the application of Liouville's theorem and other principles of classical dynamics. They are thus able to follow particles both in and out of synchronism with the accelerating rf and consequently to study the process of stacking. In this section some of the basic relationships for rf acceleration in FFAG accelerators are reviewed and certain results of the Symon-Sessler treatment are restated without proof.

In scaling FFAG accelerators, the field index k is constant everywhere and is defined as

$$k = \frac{R}{B}\frac{dB}{dR} . \tag{2.1}$$

The relative rate of change of frequency with energy is

$$\frac{E}{f_0}\frac{df_0}{dE} = \frac{(k+1)E_0^2 - E^2}{(k+1)(E^2 - E_0^2)} , \tag{2.2}$$

where E is the total energy of the particle, E_0 is the rest energy, and f_0 is the particle revolution frequency. In the Symon-Sessler

formulation canonical variables from which a Hamiltonian are derivable are W and ϕ , where

$$W = \int_{E_i}^{E} \frac{dE}{f_o(E)} \tag{2.3}$$

and ϕ is the phase of the rf voltage as the particle crosses the accelerating gap[7]. These definitions have been specialized from reference 4 to the case where the applied rf field of frequency f is localized in azimuth and where f is equal to f_o for synchronous particles.

For a sufficient applied rf voltage V , there exists a boundary in W-ϕ space within which particles execute stable phase oscillations and are accelerated. This region is referred to as a <u>bucket</u>. Fig. 1 indicates such a region in W-ϕ space together with some typical particle trajectories through this space. The equilibrium phase angle ϕ_s of particles is related to the rf voltage by

$$V_s / V = \sin \phi_s = \Gamma \tag{2.4}$$

where V_s is the voltage gain per turn of a synchronous particle, obtained from the identity

$$V_s \equiv \frac{df/dt}{f\, df_o/dE} \; . \tag{2.5}$$

The energy width of a bucket is[8]

$$\Delta E_B = f_o \Delta W_B = \left[\frac{.8\, fV}{\pi\, df_o/dE}\right]^{\frac{1}{2}} y(\Gamma), \tag{2.6}$$

where $y(\Gamma)$ is plotted in Fig. 2 and is given by

$$y(\Gamma) \cong (1-\Gamma)^{0.8} \quad . \tag{2.7}$$

In Eq. (2.6) as well as in (2.8), (2.10), and (2.11) f_o is assumed constant over the width of a bucket. This is a very good approximation in most cases of interest. In $W-\phi$ space the area of the bucket can be re-expressed as a rectangle of area $2\pi\langle\Delta W\rangle_{Av}$. The corresponding average energy spread is[9]

$$\langle\Delta E\rangle_{Av} = f_o\langle\Delta W\rangle_{Av} = \left[\frac{32\, f\, V}{\pi^3\, df_o/dE}\right]^{\frac{1}{2}} \alpha(\Gamma) \tag{2.8}$$

where $\alpha(\Gamma)$ is plotted in Fig. 2 and is given by

$$\alpha(\Gamma) \cong (1-\Gamma)^{1.7} \quad . \tag{2.9}$$

It follows that

$$\langle\Delta E\rangle_{Av} = \Delta E_B \frac{2}{\pi}\frac{\alpha(\Gamma)}{y(\Gamma)} \quad . \tag{2.10}$$

In general there is a transition energy in FFAG accelerators where df_o/dE is zero[2], however, in the experiments discussed below this energy is not reached, so that df_o/dE and df/dt are always positive.

Consider particles circulating in an FFAG accelerator with a common frequency f_o and a uniform distribution in ϕ. If an oscillator is modulated from $f \ll f_o$ to $f \gg f_o$, then these particles will not be captured by the rf, but will experience an average energy decrease of

$\langle \Delta E \rangle_{AV}$. This process is referred to as <u>rf phase space displacement</u> and is a consequence of Liouville's theorem. (The mechanism can be seen if one considers the hydrostatic analogy to phase space of an incompressible fluid in a cylindrical vessel. If an enclosed container or bucket carries fluid up from the bottom of the vessel, molecules of fluid not within the bucket will on the average be displaced downward as the bucket is pulled up past them. The average displacement is equal to the volume of the bucket divided by the cross sectional area of the cylinder.) Each particle actually experiences an energy displacement ΔE which depends on its initial location in ϕ-space so the above group of particles will display a distribution of displacements ΔE. Symon has evaluated such distributions[10] (following from the integral of Eq. (84) of reference 4) a typical example of which is shown in Fig. 3. The maximum energy displacement ΔE_M has been found as a function of Γ. It is given by

$$\Delta E_M = \langle \Delta E \rangle_{AV} / g(\Gamma) \tag{2.11}$$

where $g(\Gamma)$ is plotted in Fig. 2 and is given by

$$g(\Gamma) \cong (1-\Gamma)^{1.3} . \tag{2.12}$$

The major effects contributing to these energy displacements occur when f is close to f_0.

The process of beam stacking is simply a sequence of phase displacements. Consider the following example, taking for simplicity all pertinent

parameters as nearly constant and all processes as adiabatic (e.g. Γ almost zero), so that $\langle \Delta E \rangle_{Av} = \Delta E_M$. An rf oscillator brings up q particles and deposits them around an energy E_1, corresponding to the turn-off frequency f_1 of the oscillator. These particles will fill the region $E_1 \pm \frac{1}{2}\langle \Delta E \rangle_{Av}$ uniformly. They will be phase displaced downward an amount $\langle \Delta E \rangle_{Av}$ by the second rf pulse, another $\langle \Delta E \rangle_{Av}$ by the third, etc. so that after m subsequent rf cycles $(m+1)q$ particles will be distributed between $E_1 + \frac{1}{2}\langle \Delta E \rangle_{Av}$ and $E_1 - (m + \frac{1}{2})\langle \Delta E \rangle_{Av}$, with a density equal to that in the accelerating buckets. If the acceleration and turn-off processes are not adiabatic, particles will spread outside the above region. The extreme boundaries of the stack will be very nearly $E_1 + \frac{1}{2}\Delta E_M$ and $E_1 - (m + \frac{1}{2})\Delta E_M$, so the particle density averaged over the region will be $g(\Gamma)$ times that in the buckets. Actually for large m most of the particles will lie between E_1, and $E_1 - m\langle \Delta E \rangle_{Av}$ with a density close to that of the accelerating buckets. The exact energy distribution of particles in a stacked beam may be found by numerical integration of the equations of motion. Such a procedure is practical using digital computers and is being carried out on the MURA IBM 704 high-speed digital computer.

III. EXPERIMENTAL METHODS

The energy and revolution frequency of the electrons in the FFAG model accelerator[5] are presented in Fig. 4 as a function of the machine radius. In the original design of the accelerator, betatron acceleration was used and no provision had been made for applying the radio frequency acceleration needed for these experiments. To simplify this rf problem

three stages of acceleration are employed. First, the electrons are betatron accelerated from injection to an intermediate energy, where they are allowed to "coast"; second, rf experiments are performed by applying one or a series of frequency modulated rf pulses to the coasting beam; third, any remaining electrons are accelerated to the target with a second betatron pulse. By the use of such a procedure the rf frequency sweep can be reduced to a few Mc range, which is easily obtained. This section discusses the betatron pulses, the rf acceleration system, and the methods used for the experimental measurements.

A. Betatron Acceleration

The accelerating gap voltage which is obtained with the two pulses of the betatron core is indicated in Fig. 5a and Fig. 5b, the latter showing the portions of the waveform actually used for acceleration; injection is indicated in Fig. 5b by a spike near the peak of the first pulse. Electrons are accelerated by the first betatron pulse to the coasting energy, which is easily variable by changing the time of injection with respect to the betatron pulse. The first betatron pulse has a tail due to decay of eddy currents in the betatron core, which continues to accelerate the electrons appreciably out to about 2 milliseconds. The electrons are coasting only after this period, and rf experiments are not initiated until then. The second betatron pulse accelerates the electrons the remainder of the way to the target. The beam half life due to gas scattering can be found by varying the turn-on time of this second betatron pulse. At a beam coasting energy of 300 kv this half life is of order one millisecond at 1×10^{-6} mm Hg , so only a few millisecond

interval is available for any rf experiments to be performed between the betatron pulses.

B. Radio Frequency Acceleration

A series of frequency modulated rf pulses is required to perform beam stacking experiments on the electrons coasting after the first betatron pulse; a rapid repetition rate is necessary because of the short beam lifetime. The following section describes the methods used to obtain these pulses.

1. General Description

Fig. 6 is a photograph of the electron model with one magnet removed, showing the aluminum vacuum tank and an insulated gap. It is evident that the construction leaves little space for an rf cavity. Another method of applying rf to the particles would be the use of drift tubes inside the tank; these, however, would have a large capacity to the tank walls as well as decreasing the vertical aperture available for the beam. A third alternative, and the one used, is to apply rf directly across one of the gaps between halves of the vacuum tank without the use of an enclosing cavity. Fig. 7 is a schematic drawing of the rf oscillator and vacuum tank. A fraction of the voltage developed across the resonant circuit of the oscillator is applied to the gap through a small coupling capacitor. The inductive loop made by the vacuum tank has a reactance large compared to the highly capacitive gap. Frequency modulation is obtained by voltage polarization of ferroelectric capacitors located in the resonant circuit of the oscillator, a system employed successfully on the University of Michigan synchrotron. The required

frequency sweep is available at a repetition rate high enough to get a considerable number of pulses into the few milliseconds available. Fig. 8 shows some detected rf pulses and their beat signals with a constant frequency oscillator. Fig. 9 shows an rf pulse and the two betatron pulses, along with photomultiplier pulses from the beam. In Fig. 9b the turn-on frequency of the rf pulse is that of the coasting beam, so that some electrons are captured and accelerated to the target. The electrons not captured by the rf are subsequently accelerated by the second betatron pulse. In Fig. 9c, the rf voltage is increased, and a larger fraction of the coasting beam is captured. In Fig. 9d, the rf turn-on frequency is tuned below the coasting frequency and only a few electrons are accelerated by the rf.

2. Circuits

A diagram of the frequency-modulated rf oscillator with ferroelectric capacitors is shown in Fig. 10. It is a Colpitts type oscillator, run class C with grounded grid. The fraction of output voltage fed back to the grid is determined by the tube plate-cathode capacitance and a variable grid-cathode capacitance. The ferroelectric capacitors used in the experiments are samples from Sprague Electric Co., of nominal value 100 $\mu\mu f$, which have a capacitance decrease of about a factor of 5 as the polarizing voltage is increased to 4 kv. A 10 Mc range of frequency modulation is obtained with these capacitors in the 35 to 75 Mc region; this is more than adequate for the experiments. 1000 $\mu\mu f$ samples of K6000 material from Centralab give a factor of 10 capacity change, and a 20 Mc range can be obtained with them. One limitation of this type of system is the low Q of the ferroelectric capacitors and the low circuit reactance. Typical Q's are about 20 to 50, with the higher values at higher polarizing voltage.

A block diagram of the control circuits for the oscillator is shown in Fig. 11. The circuits are designed to produce the rapid sequence of rf pulses indicated in Fig. 8. An input pulse, delayed from injection time, generates a series of trigger pulses for a few milliseconds; each of these triggers fires the 5C22 hydrogen thyratron. The 5C22 circuit is shown in Fig. 12a. The ferroelectric capacitors, connected in parallel for the polarizing voltage, are at the supply voltage until the 5C22 fires. The circuit then starts to ring, with period and damping determined by the RLC circuit parameters. L is chosen to make the oscillation rapid (a few microsecond period) and R to make the damping short of critical, so a negative voltage appears across the thyratron after one half an oscillation and turns it off. The voltage on the tube must be negative for at least 10μsec, the deionization time of the hydrogen thyratron. The ferroelectric capacitors are then recharged to the supply voltage through a resistor. The rate of change of voltage and hence the rate of frequency modulation can be varied by changing the charging resistor or the supply voltage. A bias voltage V_b is available to minimize the time spent recharging to the voltage corresponding to the turn-on frequency of the oscillator. A sketch of the voltage applied to the ferroelectric capacitors appears in Fig. 12b. To make sure that the turn-on frequency of the oscillator is reproducible, the start of the gate pulse going to the 829B screen is determined by a discriminator, which fires when the capacitor voltage reaches a set value.

C. Measurements

Some of the quantities which need to be determined for the following experiments are the rf gap voltage V, rf frequency f, its derivative

with respect to time df/dt, and the change of electron revolution frequency per unit change in electron energy df_0/dE. The rf voltage is measured on the outside edge of the gap with a calibrated diode detector and is presented on a dual trace oscilloscope, together with the beat signal of the rf against a constant frequency oscillator, as in Fig. 8. By using the null of the beat signal, f and df/dt are easily found. Fig. 13 shows a frequency vs time curve for an rf pulse. Over the range covered the curve is accurately represented as $f = f_1(1 - e^{-\lambda t})$, where both f_1 and λ are easily varied, as mentioned earlier. Successive rf pulses repeat their FM cycles to within a few kc; the voltage also repeats quite accurately. The turn-on time of the rf pulses is one or two μsec, which is short compared to a typical phase oscillation period of 30 μsec; the turn-off time is slightly longer, of the order of 5 μsec.

The quantity df_0/dE is measured directly with the use of the second betatron pulse as follows. A Δf_0 between two different coasting energies is easily obtained by observing the two rf capture frequencies. The ΔE between these coasting energies can be found in the situation of Fig. 5 by noting the difference in the time that the electrons reach the target during the second betatron pulse. This difference in time, multiplied by the betatron voltage and electron revolution frequency (both of which are virtually constant over the time increment) equals the energy difference between the two coasting beams ΔE, determining df_0/dE. The second betatron pulse can be used in the same fashion to analyze the effects of any rf operations on the energy of the coasting electrons. It is fortunate for these experiments that the beam pattern

during the second betatron pulse reproduces quite accurately on successive cycles (at a 30 cps rate), indicating that the energy of the coasting beam and other machine parameters also reproduce accurately. Most of the power supplies are unregulated, however, and there are some slow variations in parameters.

The electron energy E can be calculated using Eq. (2.2) and the measured quantities f, df_0/dE, and k, the field index. It can also be calculated from field and radius measurements, as for Fig. 4. The latter determination of E is not as accurate as the former because of finite amplitudes of betatron oscillations and perturbations of the equilibrium orbit, effects important in FFAG accelerators because of the large field gradient and consequent rapid change of energy with radius. The two methods give results consistent within estimated errors.

IV. RF ACCELERATION EXPERIMENTS

Two experiments on ordinary rf acceleration are performed in the situation indicated by Fig. 9. The first is the experimental determination of the rf voltage necessary for beam capture, which should check with a value calculated from other experimentally measured parameters. This is essentially a test of experimental consistency. The second is finding the maximum energy spread of particles accelerated by a frequency modulated rf system, a result which can be compared directly with theoretical predictions.

A. Threshold Voltage For rf Capture

The synchronous voltage V_s (the average voltage gained per turn by captured electrons) is the threshold rf voltage for any beam capture.

This synchronous voltage is given by the identity (2.5). The quantities on the right are found by the methods of Sec. IIIc. V_s is found directly by determining the minimum rf voltage which accelerates any electrons from the coasting beam; this threshold is quite sharp and easily observed. The uncertainties in the measured quantities are estimated to be about 10%, except for f, which can be read to a few kc. The measurements and results are presented in Table I. The agreement is well inside the experimental errors.

TABLE I. Determination of rf threshold voltage. Associated machine parameters are: $h = 3.51$; electron coasting energy, 300 kv; energy at target, 365 kv; target radius, 50.3 cm in a straight section; revolution frequency at target, 73.5 Mc.

Measurements		Calculated synchronous voltage V_s volts	Measured threshold voltage V_s volts
f_0	72.2 Mc		
df/dt	16.1 kc/μsec	8.4	8.8
df_0/dE	26.6 kc/μsec		

B. Energy Spread in a Moving rf Bucket

An experimental measurement of the range of energies contained in a moving rf bucket can be made by observing the range of rf turn-on frequency over which any of the coasting beam can be captured and accelerated. From this Δf for capturing any beam, and a measurement of df_0/dE, previously discussed, a ΔE is obtained. This ΔE includes both the energy width of the capturing rf bucket and the energy width of the coasting beam. The rf voltage is turned on rapidly relative to the phase oscillation period, so that the bucket can

be assumed to appear at full size at the rf turn-on time. The maximum spread of energy of particles in a moving rf bucket can be calculated from Eq. (2.6). The experimental and calculated energy spreads for different applied rf voltages are plotted against each other in Fig. 14. In the previous experiment, Sec. IVa, the measured and calculated threshold voltages agreed well, so the zero kv point on the plot can be assumed to correspond accurately to zero bucket size. Consequently, the energy spread in the coasting beam is the intercept on the ΔE_{meas} axis, which is probably less than 1 kv. The agreement between the calculated and measured energy ranges contained in the buckets is within experimental error, the calculated values being about 15% higher than the measured.

V. EXPERIMENTS ON BEAM STACKING

The experiments of this section are designed to study the possibility of stacking beams in FFAG accelerators. The central question relating to the number of groups of particles which can be accelerated and stacked is the effect of subsequent rf sweeps on previously deposited beam. The theory discussed in Sec. II gives a very definite prediction: as an rf bucket sweeps up through a previously deposited coasting beam the average energy of this coasting beam is lowered by just the average energy spread of the bucket. As a consequence, if full buckets are brought up and stacked, the particle density can be made almost the same as that of the incoming buckets. This predicted phenomenon of phase displacement is quantitatively tested in Sec. Va. In Sec. Vb there is a qualitative demonstration of beam stacking, where the coasting beam is transferred to a higher energy with a series of rf sweeps.

A. Experimental Tests of Phase Displacement

Two methods are used to observe the effect of a frequency modulated rf pulse on the energy of the coasting beam. The first method uses a betatron pulse and the second uses rf pulses to determine any energy shifts due to the applied rf. The average energy decrease of the coasting beam is predicted by Eq. (2.8) and the maximum energy decrease of any of the electrons by Eq. (2.11).

1. Second Betatron Pulse Detection

One or more rf sweeps are made to operate on the beam coasting between the two betatron pulses, as in Fig. 9, and any energy shift is measured with the aid of the second betatron pulse. This test is pictured in Fig. 15, where two identical rf pulses are used, each long enough to accelerate any captured electrons to just short of the target energy. Fig. 15a shows the second betatron pulse on an expanded scale. In Fig. 15b the rf pulses are turned on with starting frequency above that of the coasting electrons, and do not affect the beam appreciably; it appears at the same time as without the rf pulses. The time spread of the photomultiplier pulse could be due to either an energy spread of about 15 kv or a spread in radial betatron oscillation amplitudes of about 4 mm. Since the energy spread has been shown in Sec. IVb to be less than one kv, the observed width must be due to the different oscillation amplitudes present. In Fig. 15c the starting frequency of the rf pulses is adjusted down to the coasting electron frequency so that a large fraction of the beam is captured and accelerated to a higher energy; this beam appears during the second betatron pulse together with the uncaptured beam. In Fig. 15d the rf starting frequency is moved below that of the coasting electrons, so that the rf pulses frequency modulate through the coasting beam fre-

quency. The rf captures only a trace of beam. The uncaptured coasting beam, accelerated to the target by the second betatron pulse, hits the target later than it does with no rf present, so there has been a measurable decrease in energy of the coasting beam by the upward passage of the rf buckets through the coasting beam frequency. The maximum energy loss of the electrons, measured by observing the time shift in the right hand edge of the pulse, is larger than the average loss.

Quantitative measurements of the time shifts of the beam are made directly from the oscilloscope, and are estimated to be accurate to about 10%. Experiments with different numbers of rf buckets indicate that the average and peak displacements are proportional to the number of buckets, although the pulse pattern changes shape considerably with additional sweeps. Resultant energy displacements for a set of runs made with two rf sweeps are presented in Table II, along with the theoretically calculated displacements, from Eqs. (2.8) and (2.11). The measured and

TABLE II. Phase displacement with two rf pulses, using betatron detection. Experimental conditions are as in Table I.

Rf peak volts			Energy loss per rf sweep		
			Maximum	Average	Ratio
V	Γ		ΔE_M kv	$\langle \Delta E \rangle_{Av}$ kv	$1/g(\Gamma)$
42.5	.196	Measured	7.6	6.2	1.23
		Calculated	9.9	7.4	1.35
28	.30	Measured	5.7	3.8	1.50
		Calculated	7.8	4.9	1.59

calculated displacements appear to be in rough quantitative agreement, the calculated values being consistently about 30% higher than the measured. The ratios between the maximum and average displacements are in good agreement with the theory, as well as the variation of the displacements with rf voltage. The systematic 30% difference is within experimental error.

2. Rf Pulse Detection

A second method of detecting energy shifts is to use the rf pulses rather than the second betatron pulse. This method is presented in Fig. 16 where two identical rf pulses are used. The rf sweeps are long enough to accelerate any captured electrons to the target. The beat frequency patterns of the rf pulses with the constant frequency oscillator are presented together with the photomultiplier beam pulses. In Fig. 16a the starting frequency of the rf is well above the electron coasting frequency and no beam is accelerated. In Fig. 16b the starting frequency is moved down to be slightly above the coasting frequency; some beam is picked up by the second rf pulse, as expected because of disturbances caused by the first pulse. At a slightly lower frequency, Fig. 16c, the first pulse picks up the beam. At a still lower turn-on frequency, in Fig. 16d, the beam is captured mostly by the second pulse, rather than the first, indicating the first pulse has displaced the coasting beam downward in energy to where it could be captured by the second pulse. The turn-on frequency shift from capturing by the first pulse to capturing by the second is quite considerable, far more than any possible turn-on frequency differences between the two rf pulses, or changes in frequency of the coasting beam from other causes. From this measurement of Δf, and measurement of df_0/dE, a ΔE is obtained. This ΔE, from tuning for maximum picked-up beam, can be anywhere from the average displacement to the maximum displacement. As in the previous experiment, ΔE is proportional to the number of rf sweeps displacing the beam. The measured frequency shifts are estimated to be accurate to about 10%. Results with three rf pulses, two displacing and one detecting, are presented

in Table III, together with theoretically calculated values. The measured

TABLE III. Phase displacement by two rf pulses, using rf pulse detection. Conditions are as in Table I, except that df/dt is 13 kc/μsec instead of 16 kc/μsec.

Rf peak volts V	Γ		Energy loss per rf sweep Maximum ΔE_M kv	ΔE kv	Average $\langle \Delta E \rangle_{Av}$ kv
42.5	.155	Measured		8.0	
		Calculated	9.9		7.9
28	.245	Measured		6.2	
		Calculated	7.8		5.4

displacements are consistent both with the calculated values and the measured values of the previous experiment. This consistency is evidence that most of the energy displacement process occurs when f is close to f_o, since the rf in this experiment is turned on only slightly below f_o.

B. Demonstration of Beam Stacking

The mechanism of beam stacking can be shown by transferring the coasting beam to a higher energy with a series of identical rf pulses. This situation is presented in Fig. 17, a photograph taken during the period of the second betatron pulse; it is similar to Fig. 15. The rf voltage is low, to keep the buckets small, and the turn on frequency is detuned to prevent the beam from being entirely captured on the first rf pulse. In Fig. 17a there are no rf pulses present; Fig. 17b has one, Fig. 17c two, Fig. 17d three, and Fig. 17e, four. The coasting beam is transferred to the higher energy by the successive rf pulses, the later pulses displacing the previously deposited beam downward in energy, as expected from the theory and the experiments of Sec. Va. There is very little increase in energy at the top of the stack, as predicted by the theory. If the low energy coasting

beam were replenished after each rf pulse, the situation corresponding to rf acceleration from injection, the transferred pulse in Fig. 17e could be expected to be almost four times as large as indicated. Fig. 18 is similar to Fig. 17, except that the rf is at maximum voltage and more pulses are used. Fig. 18a has no rf pulses, Fig. 18b one, Fig. 18c four, Fig. 18d seven, and Fig. 18e ten. Most of the beam is picked up by the first pulse, and practically all by four pulses. As in the previous case, the stacked beam is phase displaced downward by the successive rf pulses with an increasing spread in energy. After seven pulses the maximum displaced beam has been moved down to the original starting energy; it is subsequently captured and transferred up again, as indicated in Fig. 18e.

VI. CONCLUSIONS

The quantitative measurements of energy spread in an rf bucket and energy displacement of stacked particles by a frequency modulated rf pulse are in satisfactory agreement with the theory. A qualitative demonstration of the stacking process shows a general particle behavior which also agrees with theoretical predictions. Thus the effects of rf voltage on particle energy seem to be reasonably well understood and as far as rf acceleration processes are concerned, successive beam pulses can be stacked with a particle density approaching that of the accelerating buckets. This density may be limited, of course, by other mechanisms not discussed here, such as the effects of space charge and rf excitation of betatron oscillations.

ACKNOWLEDGMENTS

It is a pleasure to acknowledge many helpful discussions about these experiments with K.R. Symon and other members of MURA. We also wish to thank G. Edict of the University of Michigan synchrotron project for useful suggestions on the rf circuitry and D. Ford for his help in constructing the circuits.

REFERENCES

1. D. W. Kerst, et al., Phys. Rev. 102, 590 (1956).

2. Symon, Kerst, Jones, Laslett, and Terwilliger, Phys. Rev. 103, 1837 (1956).

3. F. S. Crawford and W. F. Stubbins UCRL - 3463 (1956) (unpublished).

4. K. R. Symon and A. M. Sessler, Proceedings of the CERN Symposium on High Energy Accelerators and Pion Physics (CERN, Geneva, 1956) Vol. 1, p.44.

5. Cole, Haxby, Jones, Pruett, and Terwilliger, Rev. Sci. Instr. 28, 403 (1957).

6. D. Bohm and L. Foldy, Phys. Rev. 70, 249 (1946). T. R. Kaiser, Proc. Phys. Soc. A LXIII, 52 (1950). E. D. Courant, M. S. Livingston, and H. S. Snyder, Phys. Rev. 88, 1190 (1952).

7. The variable ϕ as defined here is related to the corresponding variable φ of reference 4 by $\phi = \pi - \varphi$.

8. From Eqs. (41), (44), and (79) of reference 4.

9. From Eq. (80) of reference 4.

10. We wish to thank Dr. Symon for the use of these results prior to publication.

FIGURE CAPTIONS

Fig. 1 A region of W-ϕ phase space showing a phase stable region, or "bucket" (shaded). The bucket width, ΔW_B, and average width, $\langle \Delta W \rangle_{Av}$, are indicated. Curves indicate possible trajectories of particles in $W-\phi$ space.

Fig. 2 The functions $y(\Gamma)$, $\alpha(\Gamma)$, and $g(\Gamma)$ plotted vs. Γ.

Fig. 3 The density in W-space, $\rho(W)$, vs. W, of particles after a phase displacement by a moving bucket of $\Gamma = 0.5$. The particles had initially the same W value, W_0, and a uniform distribution in ϕ. The maximum and average phase displacements, ΔW_M and $\langle \Delta W \rangle_{Av}$, are indicated. The abscissa and ordinate scales are arbitrary.

Fig. 4 Calculated electron energy and revolution frequency as a function of radius.

Fig. 5 Oscilloscope photograph of method of obtaining electrons coasting at an intermediate energy. Time scale 500 μsec/cm.

a. Betatron waveform, 10v/cm.

b. Portion of waveform used for acceleration, injection time indicated by a spike near peak of first pulse. 5v/cm.

c. Photomultiplier pulse from beam striking target after acceleration by second betatron pulse.

Fig. 6 Photograph of the electron model with one magnet removed showing vacuum tank and an insulated gap.

Fig. 7 Schematic drawing of the method of applying rf to the vacuum tank.

Fig. 8 Oscilloscope photographs of rf pulses.

a. Pulse from a diode detector on the rf gap. The time scale is 50 μsec/cm. The maximum voltage is about 45 volts.

b. Beat frequency patterns of the above rf pulse with a signal generator.

c. & d. Detector signal and beat frequency pattern from a group of rf pulses. The time scale here is 200 μsec/cm.

Fig. 9 Photographs of a frequency modulated rf pulse operating on the coasting beam between the two betatron pulses. Time scale is 500 μsec/cm.

a. Betatron and rf pulses.

b. Photomultiplier pulses from beam striking target. The turn on rf frequency is tuned for beam capture at the coasting electron frequency. The rf is 14 volts peak.

c. As in b, only the rf is raised to 46 volts, capturing more beam.

d. As in c, only the turn on rf frequency is below the coasting electron frequency.

Fig. 10 Frequency modulated oscillator circuit diagram.

Fig. 11 Block diagram of control circuits for rapid pulsing of the frequency modulated oscillator.

Fig. 12 a. Circuit for generating the high voltage polarizing pulse for the ferroelectric capacitors.

b. Voltage on the capacitors as a function of time.

Fig. 13 Measured oscillator frequency as a function of time for an rf pulse.

Fig. 14 Plot of calculated energy spread in a bucket versus a measured energy spread. The latter includes both beam and bucket. The parameter df/dt is not exactly the same for the different points, but varies from about 14 to 17 kc/μsec with changing rf voltage. The applied rf voltage went from 11.5v to 46.4v, peak values. Other parameters are as in Table I.

Fig. 15 Photograph showing phase displacement using betatron detection. The situation is similar to Fig. 9, with two identical rf sweeps, except the rf does not accelerate captured electrons all the way

to the target. Rf is 45 volts peak and the time scale is 20 μsec/cm.

a. Second betatron pulse at 5v/cm.

b. Photomultiplier pulse of beam striking target with rf starting frequency above the electron coasting frequency.

c. Rf starting frequency tuned to coasting frequency, so most of the beam is rf accelerated to a high energy and comes out early in the second betatron pulse.

d. Rf starting frequency below the coasting frequency. Only a little beam is captured and the rest is displaced later in the second betatron pulse.

Fig. 16 Photograph showing phase displacement using rf pick-up detection. Situation as in Fig. 9, with two identical rf pulses. Time scale is 100 μsec/cm. Beat frequency patterns between the rf pulses and a constant frequency rf generator are shown along with the photomultiplier pulses.

a. Rf starting frequency well above the coasting frequency.

b. Rf starting frequency just slightly above the coasting frequency.

c. Rf starting frequency equals the coasting frequency and the beam is captured by the first pulse.

d. Rf starting frequency is below the coasting frequency and the beam is captured by the second pulse, indicating the first pulse has caused a decrease in energy of the coasting beam.

Fig. 17 Photograph demonstrating beam stacking. Situation is as in Fig. 15. Rf is 10 volts.

a. No rf pulses.

b. One rf pulse, capturing beam.

c. Two rf pulses identical to the one in b.

d. Three rf pulses.

e. Four rf pulses.

Fig. 18 Photograph showing beam stacking and phase displacement. Situation is as in Fig. 17, with a time scale of 25 μsec/cm. Rf is 45 volts. The second betatron pulse has been delayed out to 5msec to permit a large number of rf pulses.

a. No rf pulses.

b. One rf pulse, capturing beam.

c. Four rf pulses, identical to the one in b.

d. Seven rf pulses.

e. Ten rf pulses.

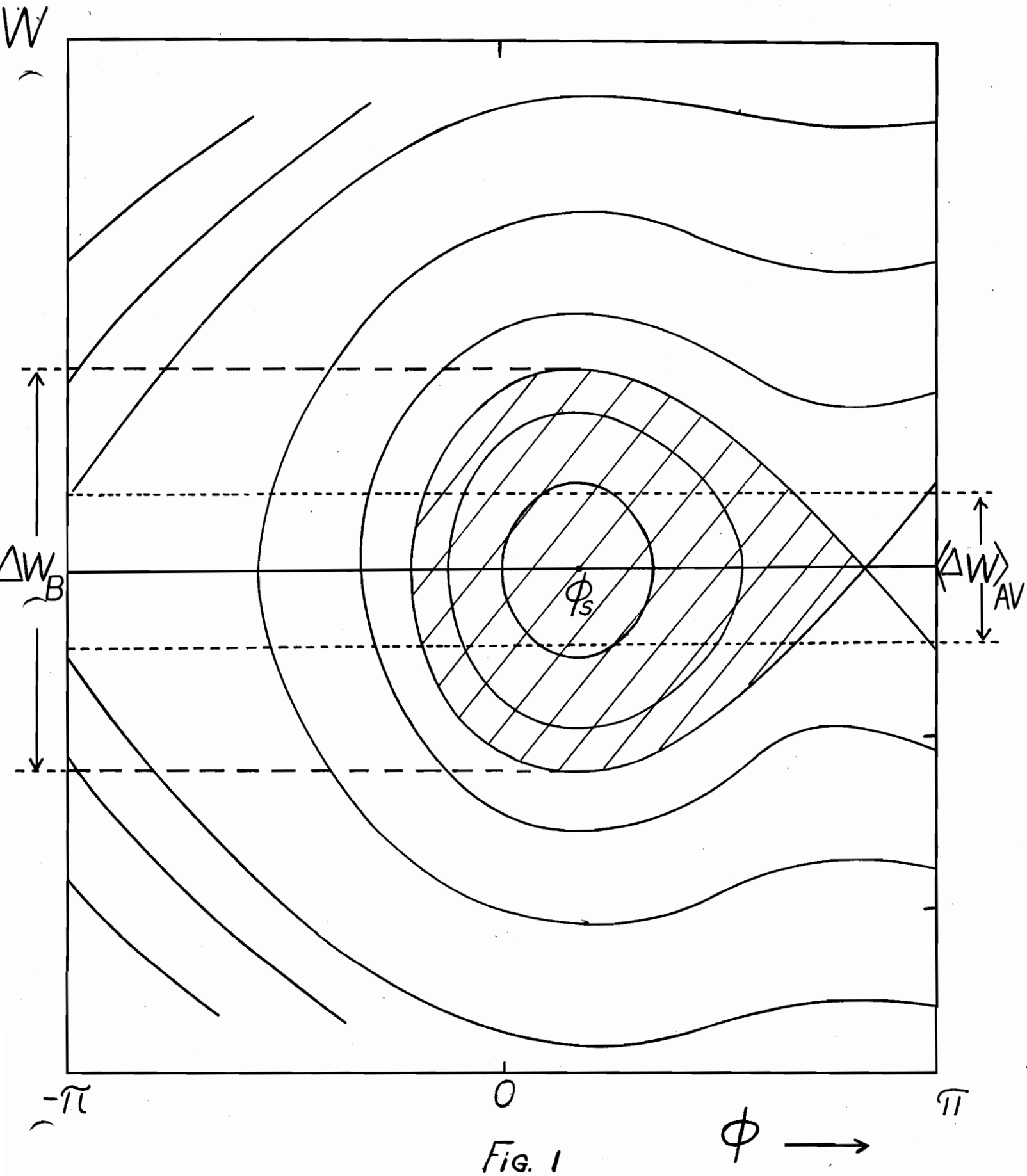

FIG. 1

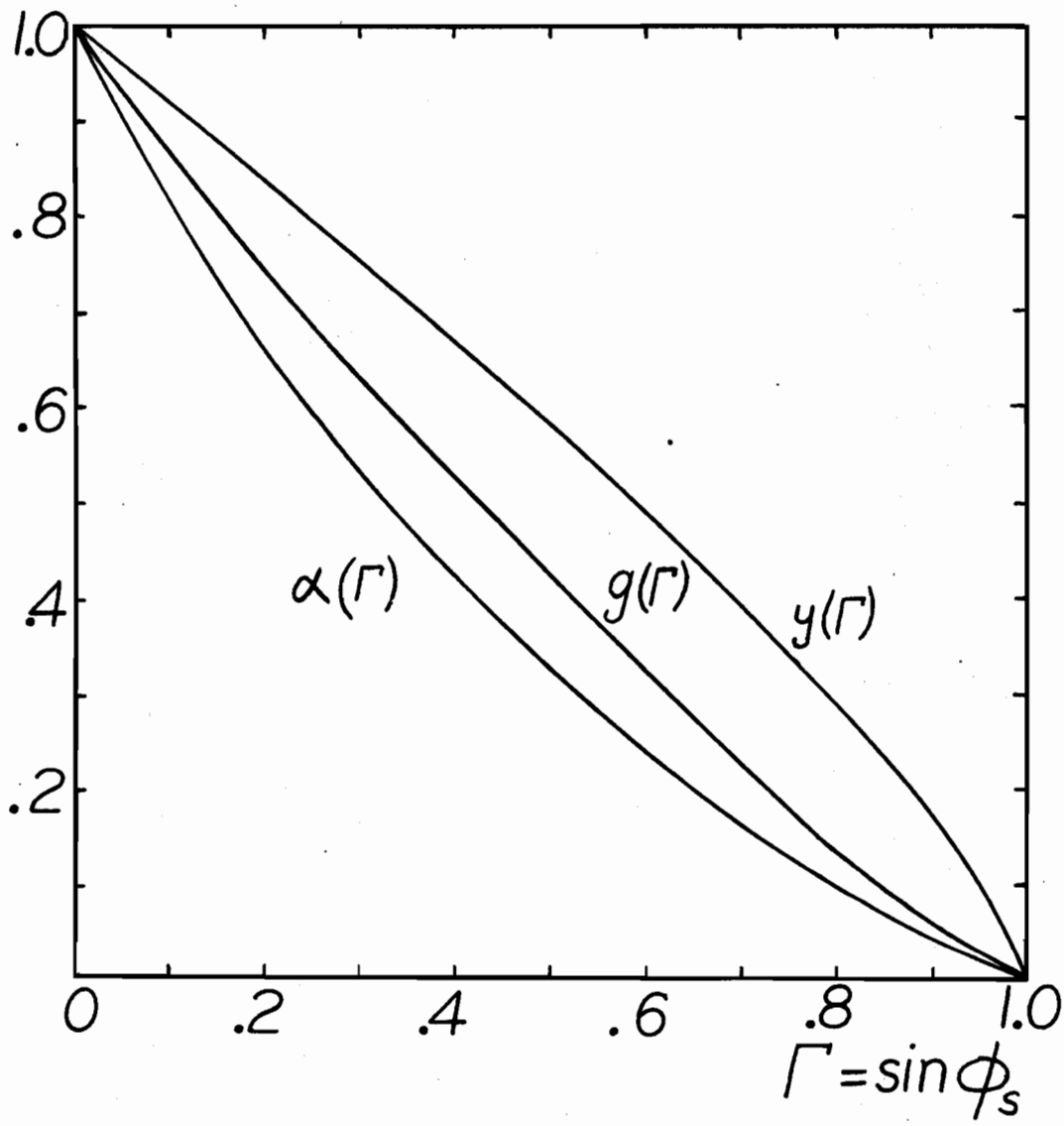

FIG. 2

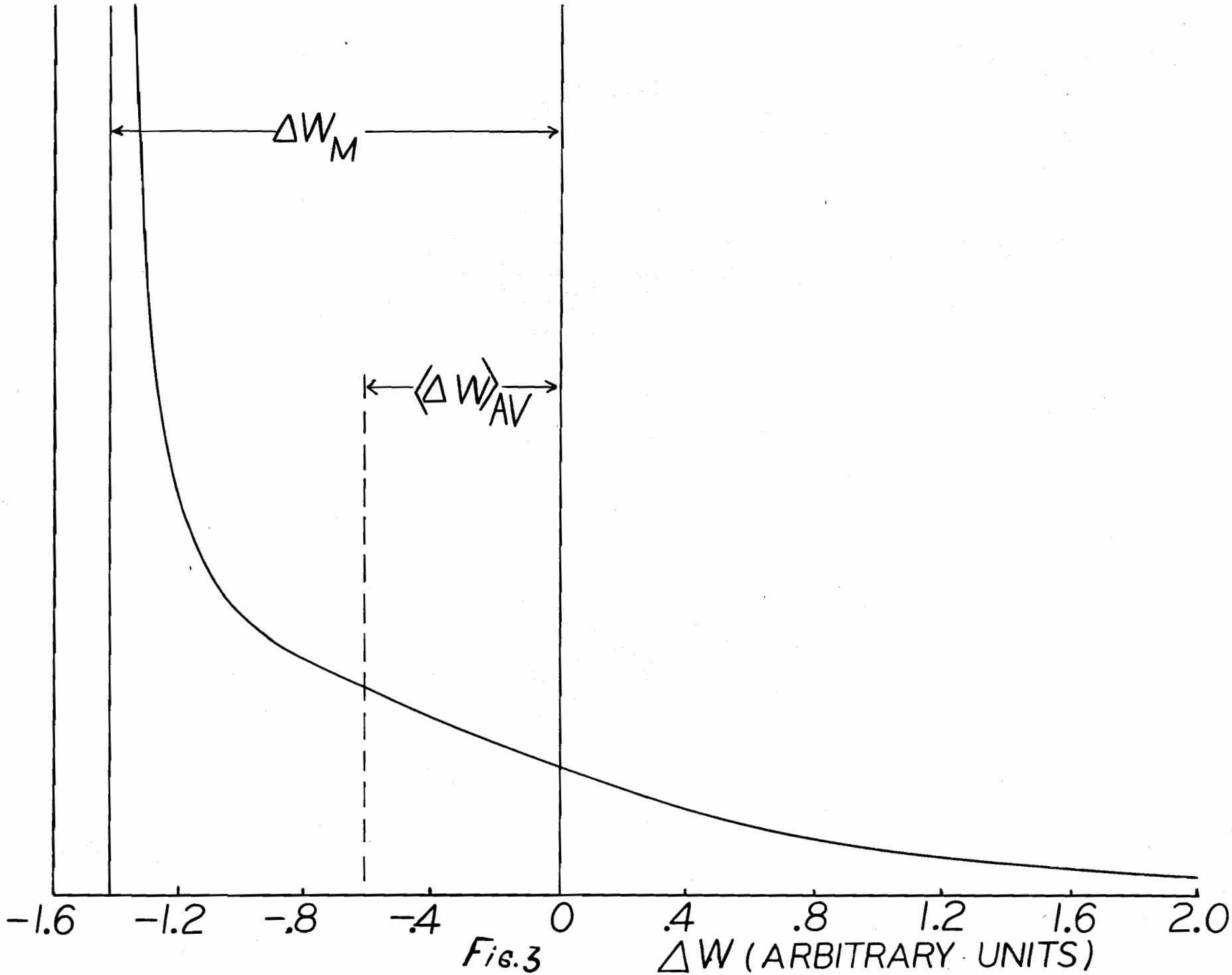
ΔW_M
$\langle \Delta W \rangle_{AV}$
-1.6
-1.2
-.8
-.4
0
.4
.8
1.2
1.6
2.0
ΔW (ARBITRARY UNITS)

Fig. 3

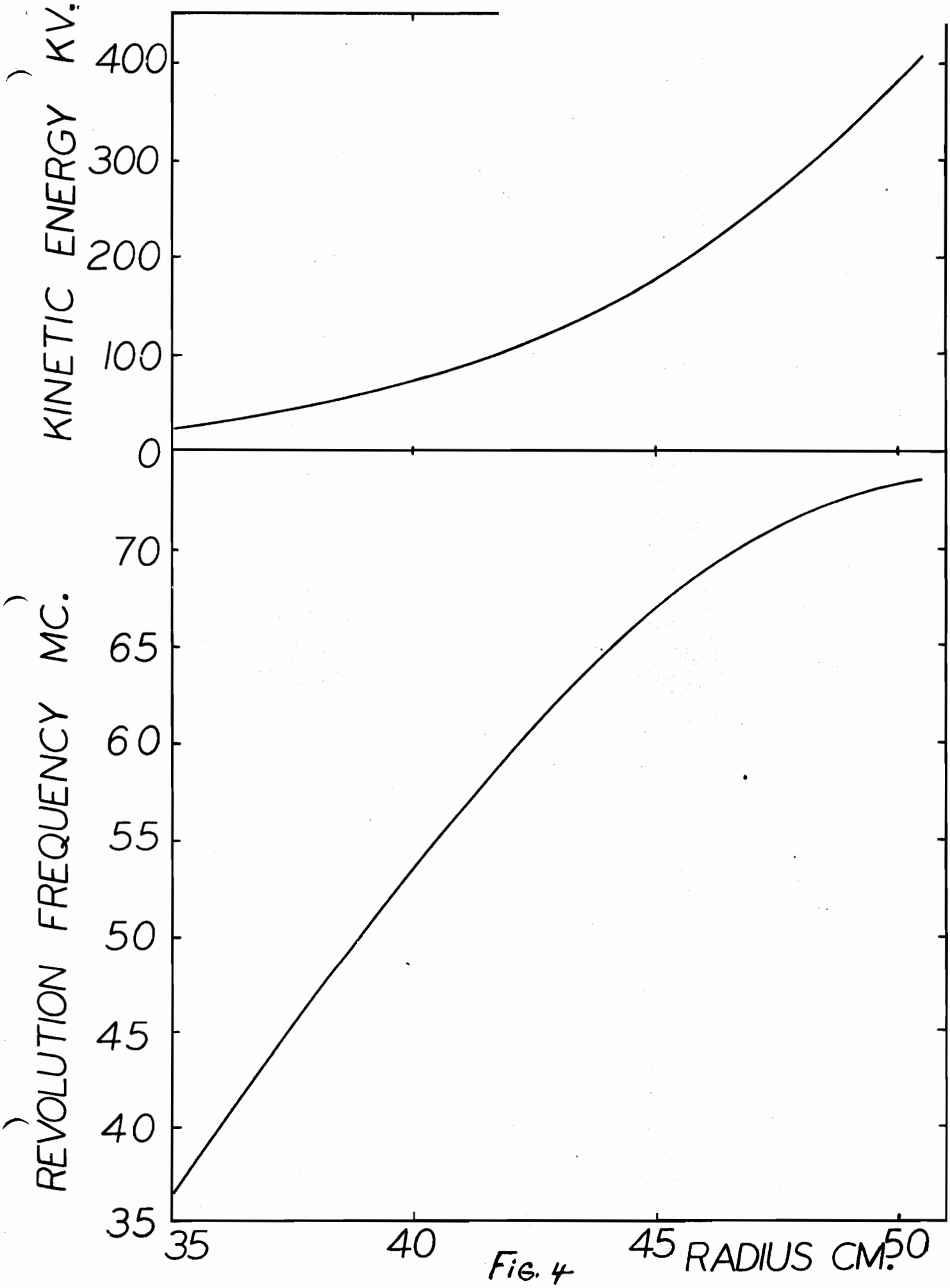
KINETIC ENERGY KV.
400
300
200
100
0
REVOLUTION FREQUENCY MC.
70
65
60
55
50
45
40
35
35
40
45
50
RADIUS CM.

Fig. 4

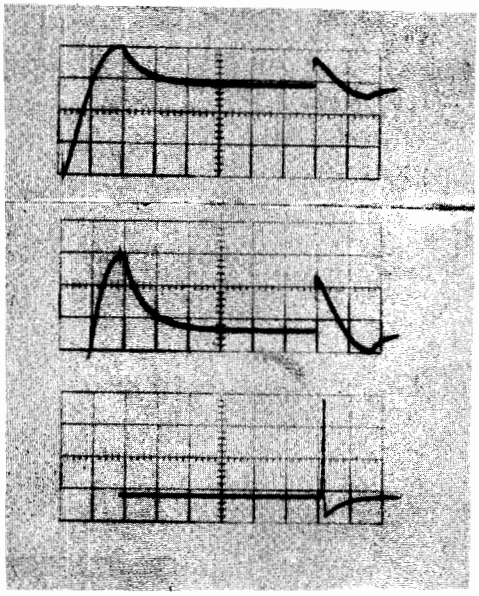

Fig. 5

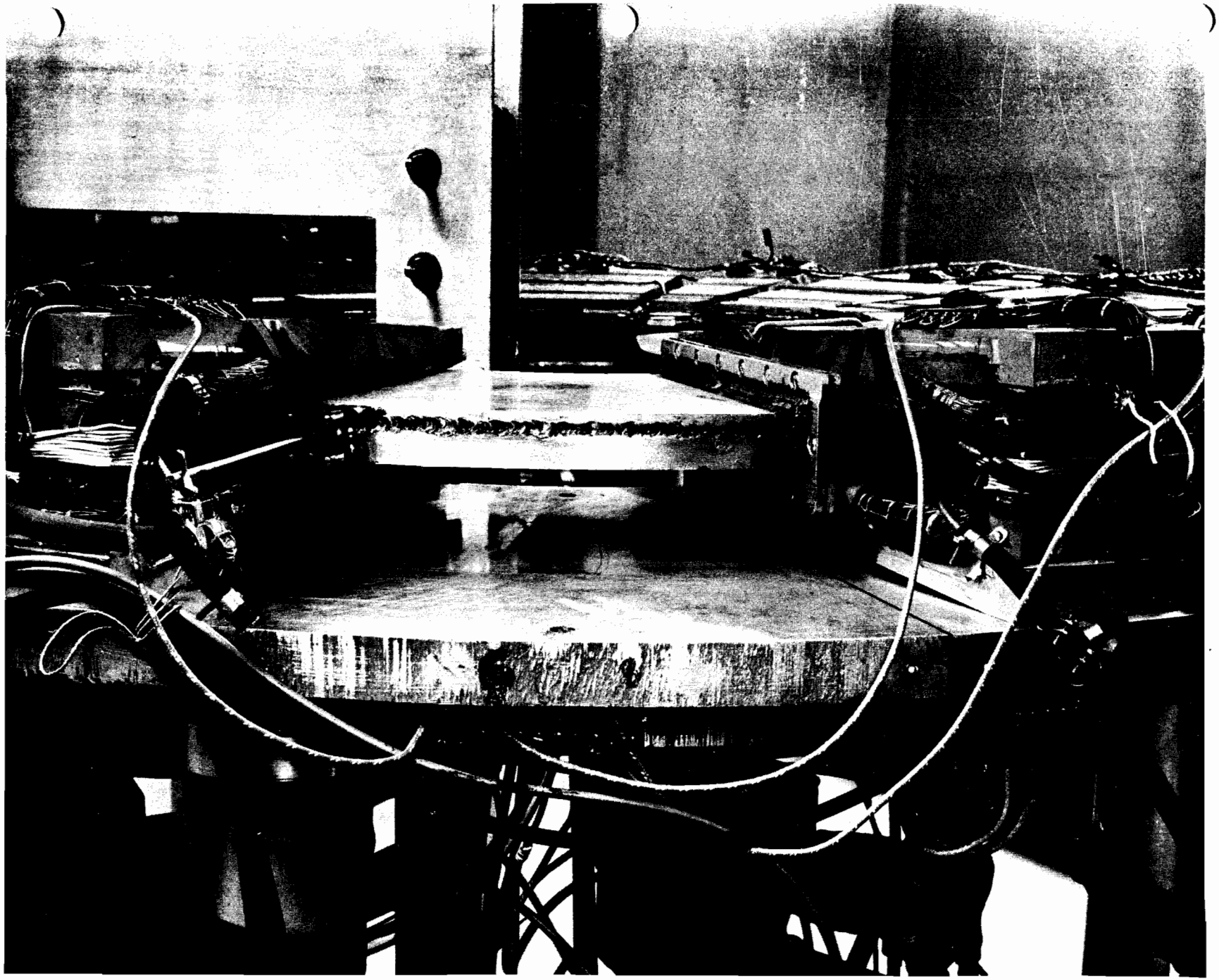

Fig. 6

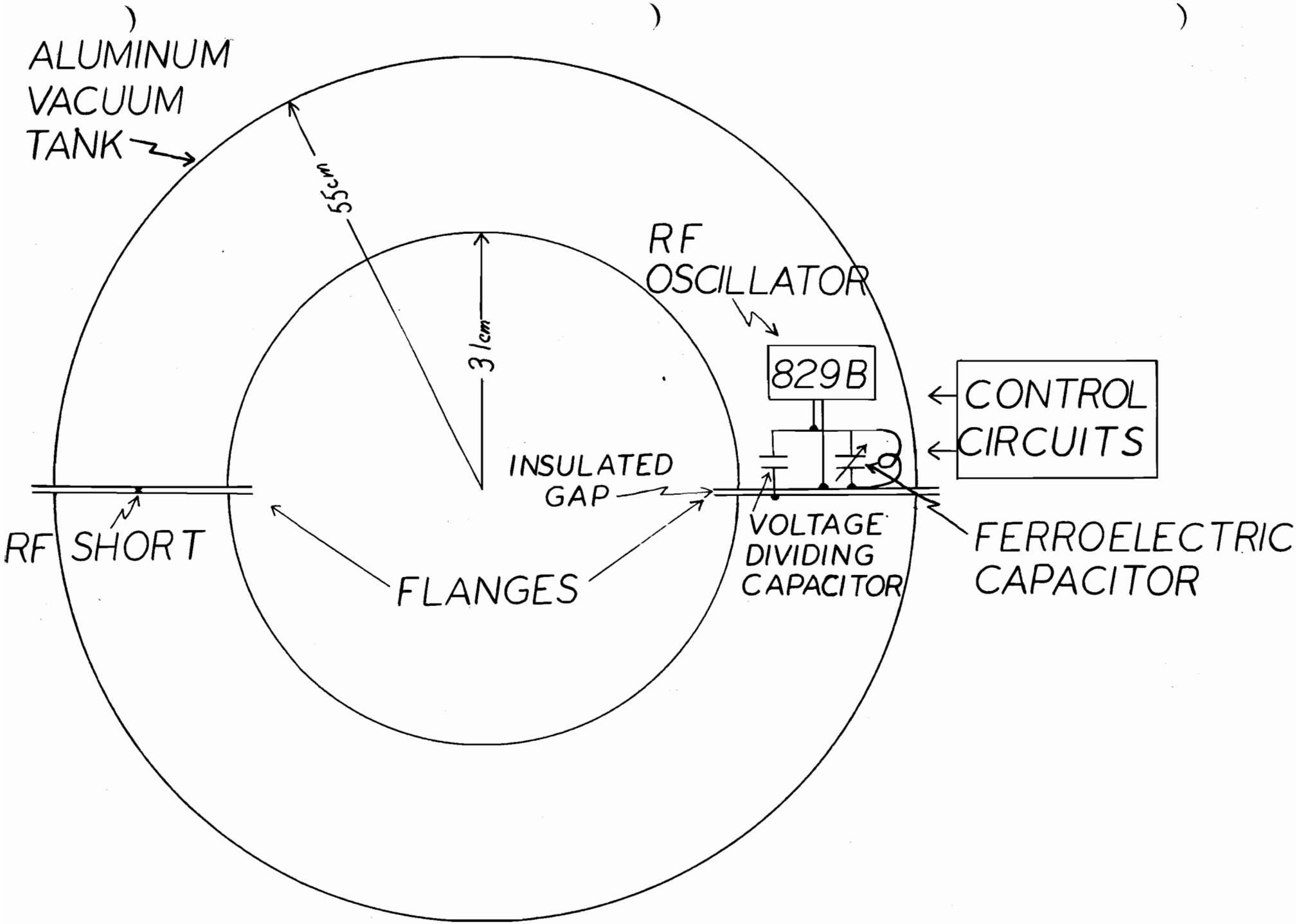
ALUMINUM
VACUUM
TANK
55cm
31cm
RF
OSCILLATOR
829B
CONTROL
CIRCUITS
INSULATED
GAP
RF SHORT
FLANGES
VOLTAGE
DIVIDING
CAPACITOR
FERROELECTRIC
CAPACITOR

Fig. 7

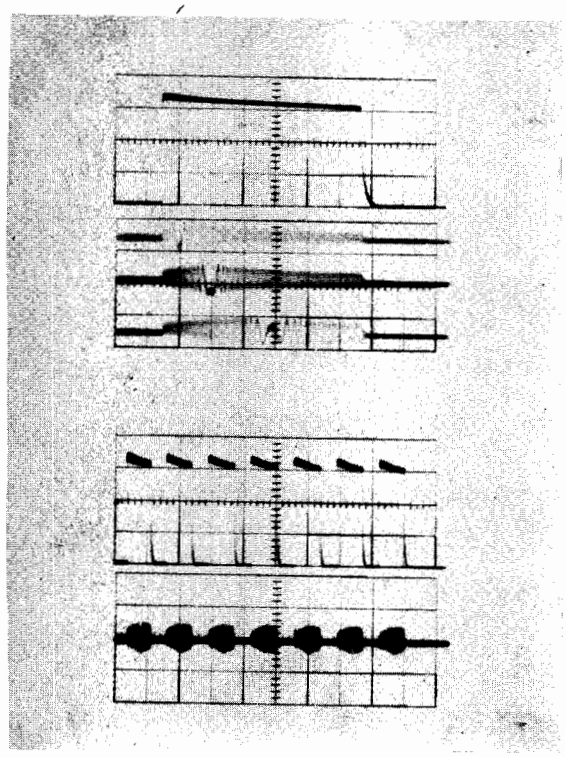

Fig. 8

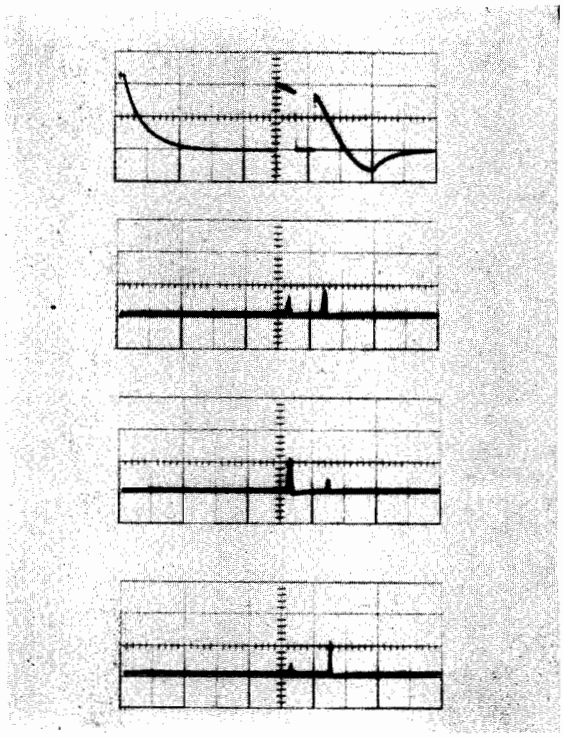

Fig. 9

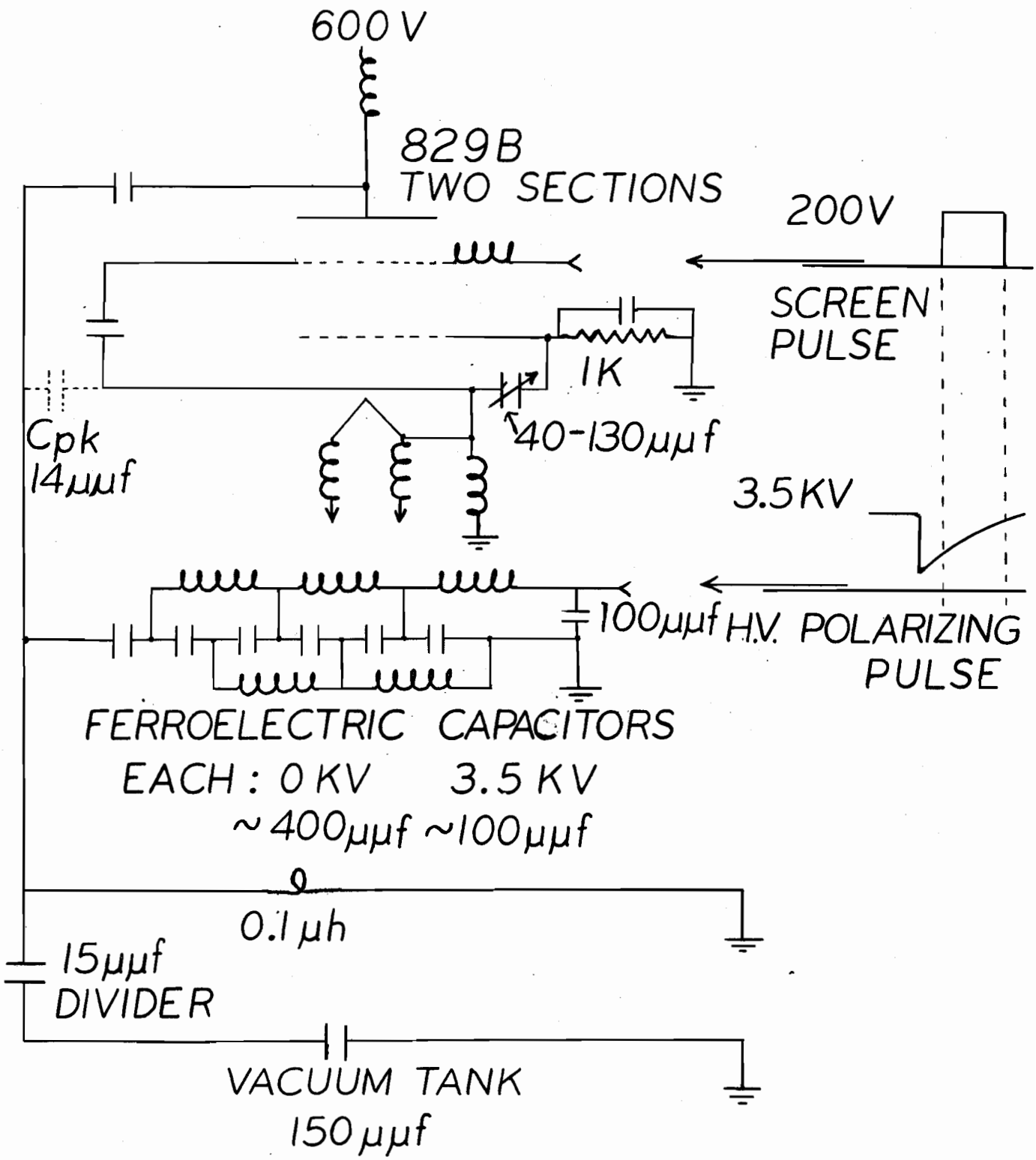
600 V
829B
TWO SECTIONS
200V
SCREEN
PULSE
1K
40-130μμf
Cpk
14μμf
3.5KV
100μμf
H.V. POLARIZING
PULSE
FERROELECTRIC CAPACITORS
EACH : 0 KV 3.5 KV
~400μμf ~100μμf
0.1 μh
15μμf
DIVIDER
VACUUM TANK
150 μμf

Fig. 10

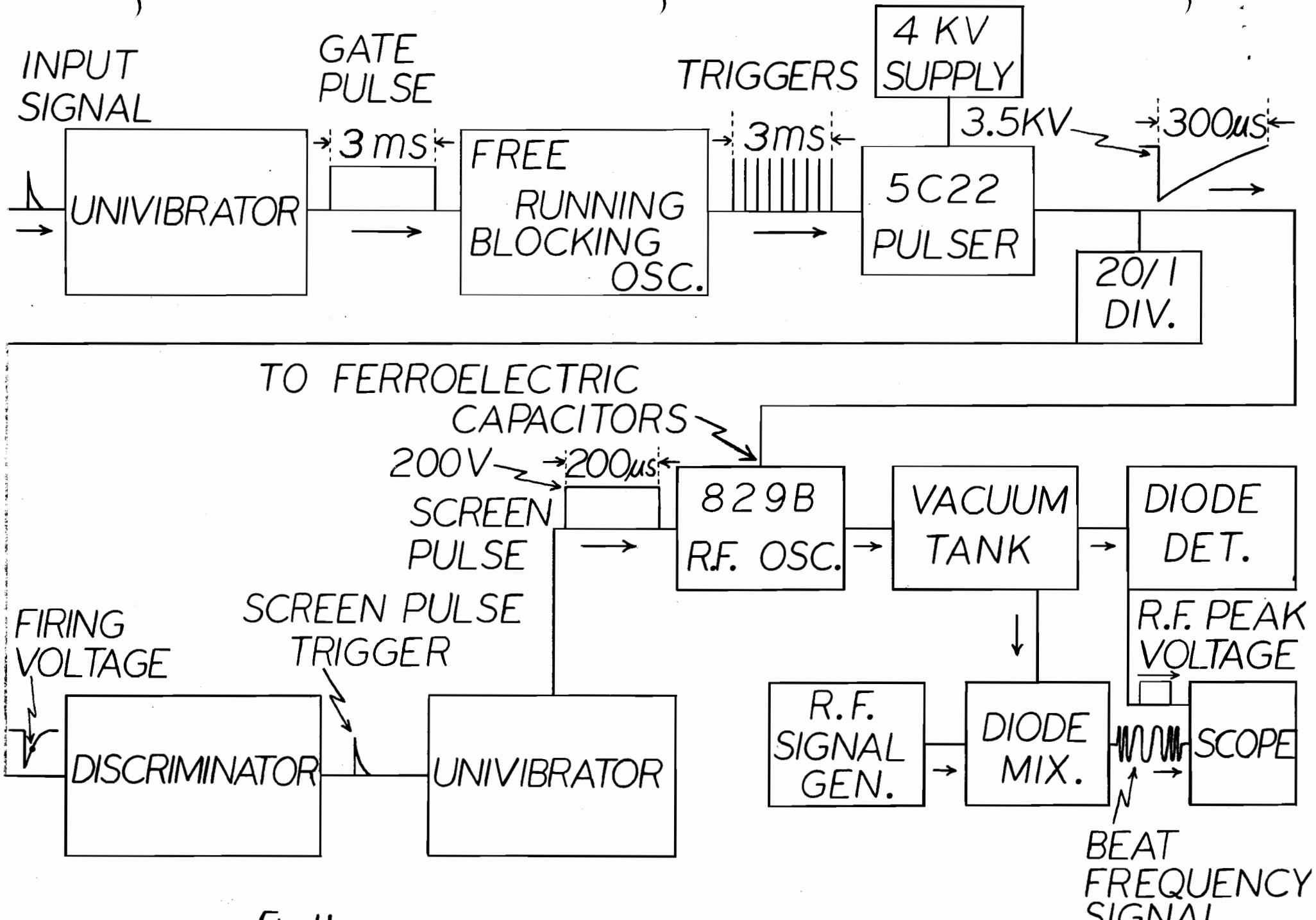

Fig. 11

ALL PARAMETERS VARIABLE

a

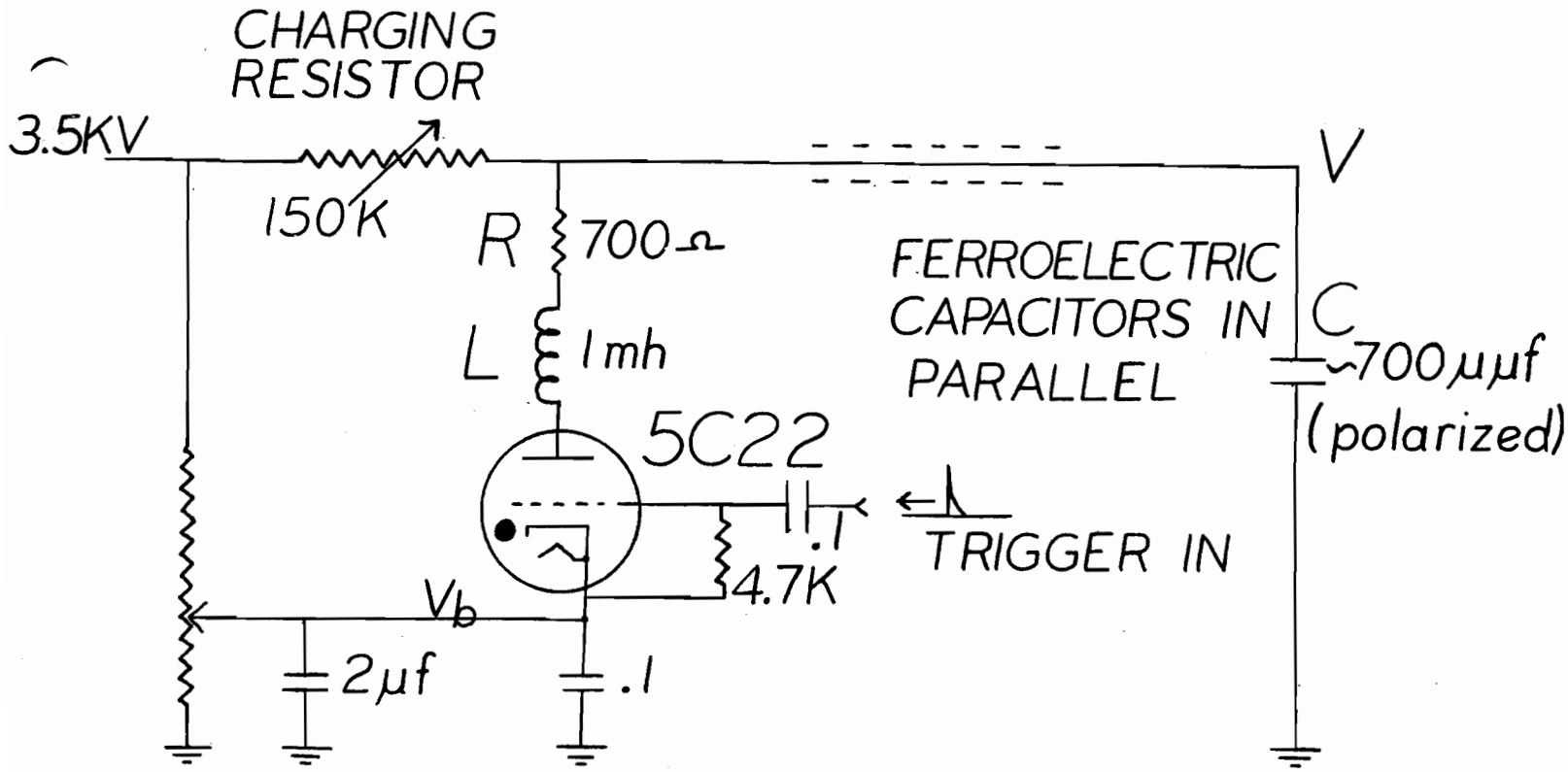
CHARGING
RESISTOR
3.5KV
150K
R
700Ω
L
1mh
5C22
V
FERROELECTRIC
CAPACITORS IN
PARALLEL
C
~700μμf
(polarized)
.1
TRIGGER IN
4.7K
Vb
2μf
.1

b

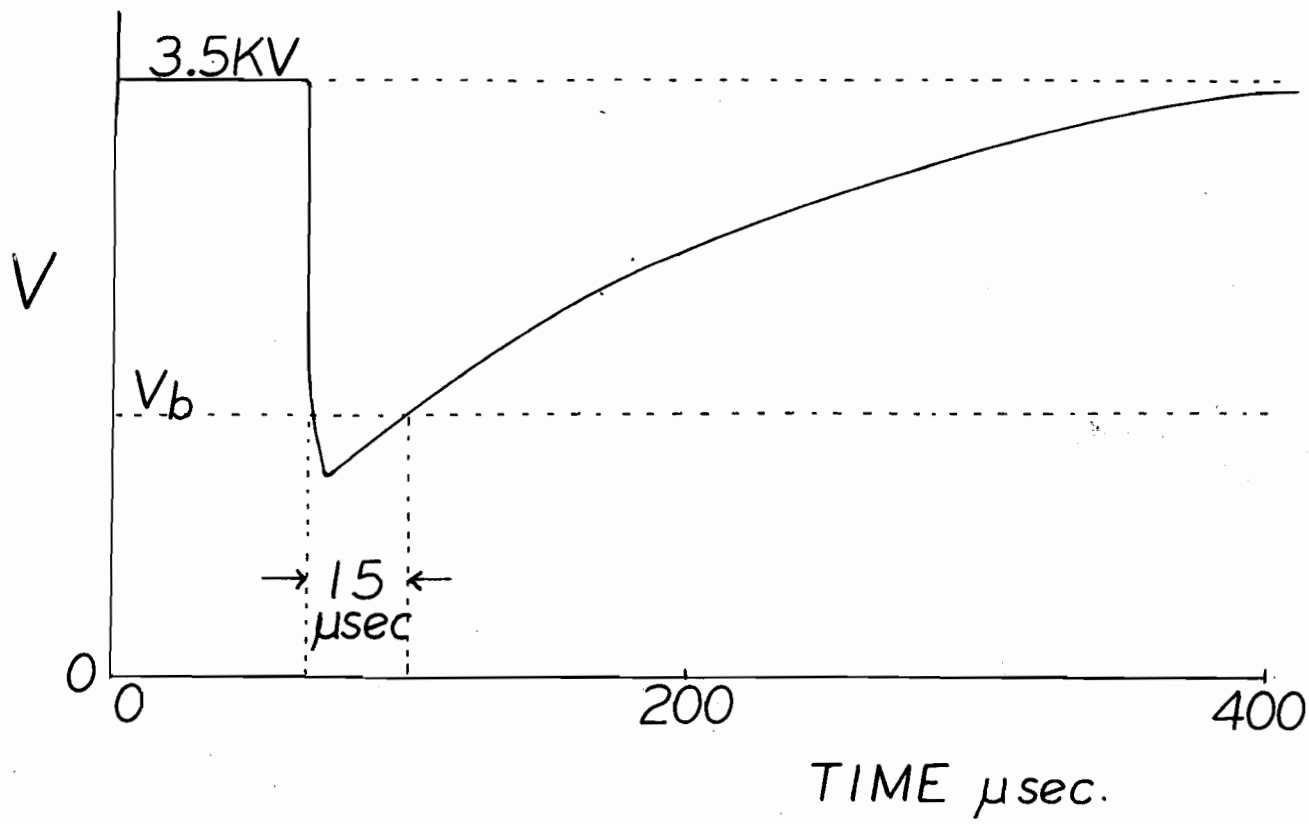
3.5KV
V
Vb
15
μsec
0
0
200
400
TIME μsec.

Fig. 12

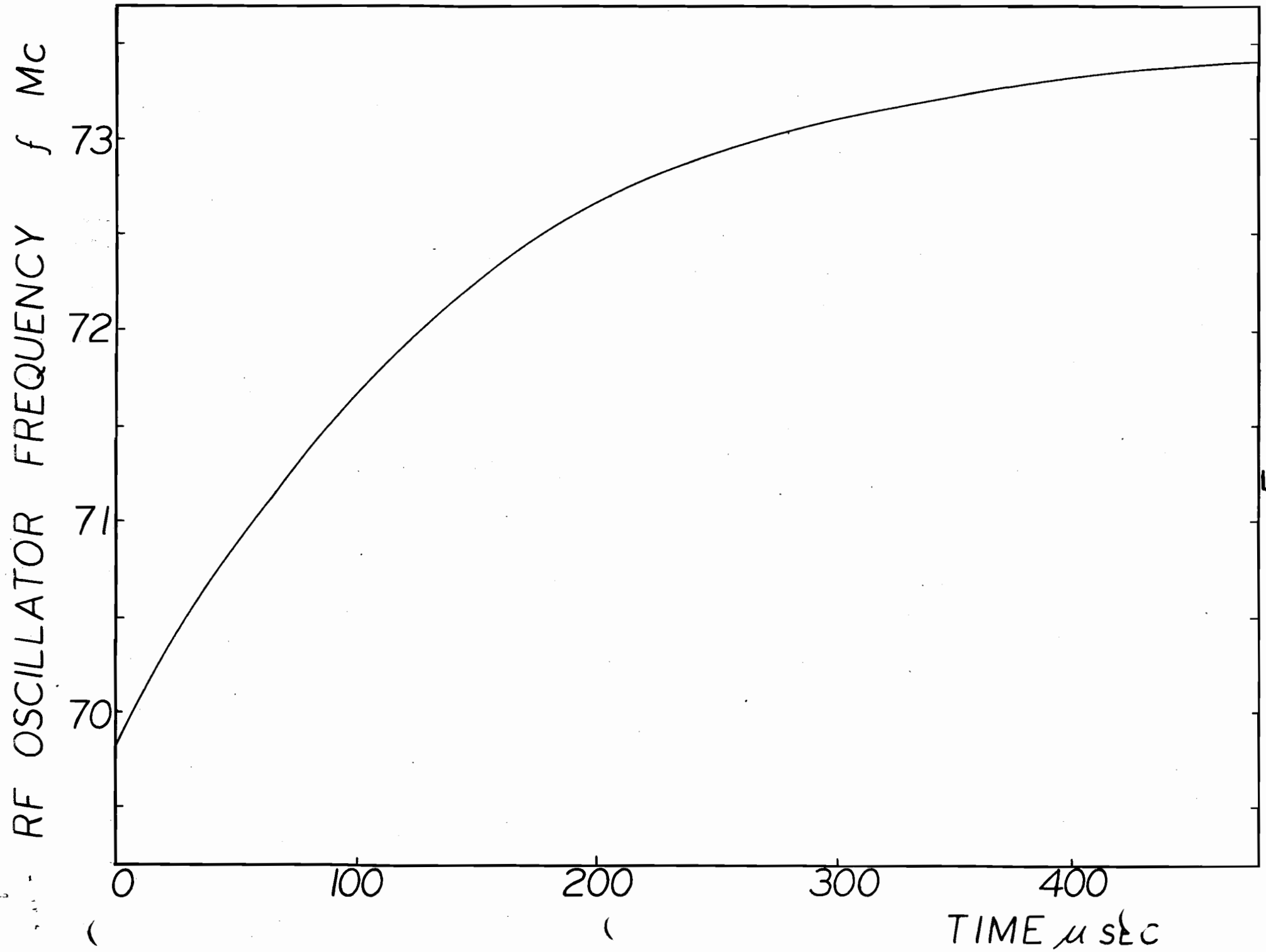
RF OSCILLATOR FREQUENCY f Mc
73
72
71
70
0
100
200
300
400
TIME μ sec

FIG 13

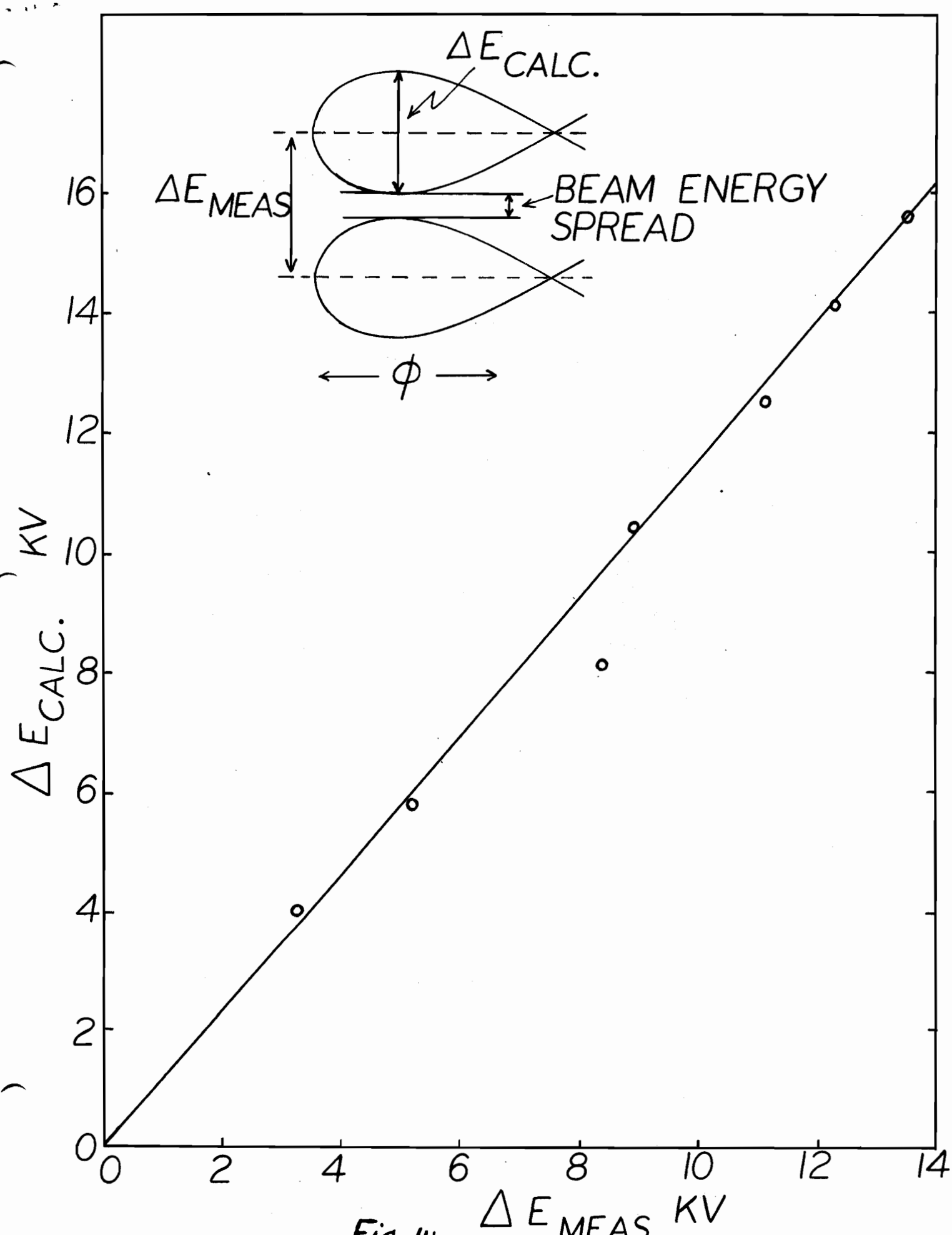
ΔE CALC.
ΔE MEAS
BEAM ENERGY SPREAD
φ
ΔE CALC. KV
ΔE MEAS KV
0
2
4
6
8
10
12
14
16

Fig. 11

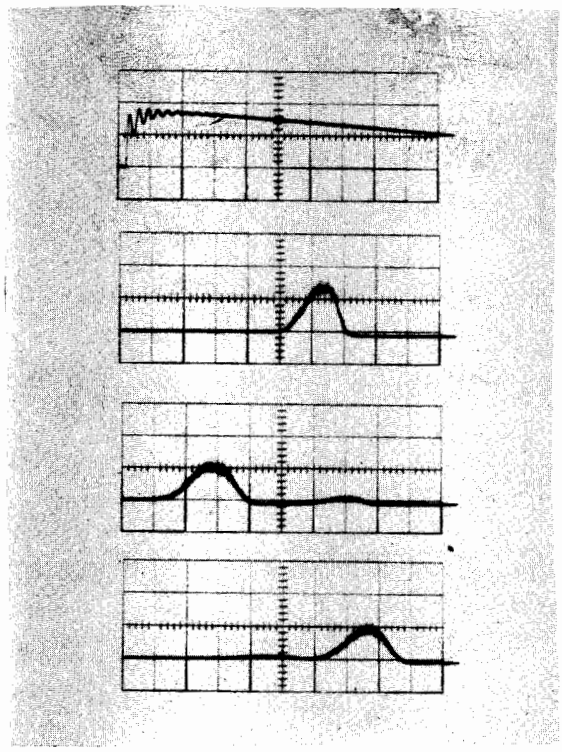

Fig. 15

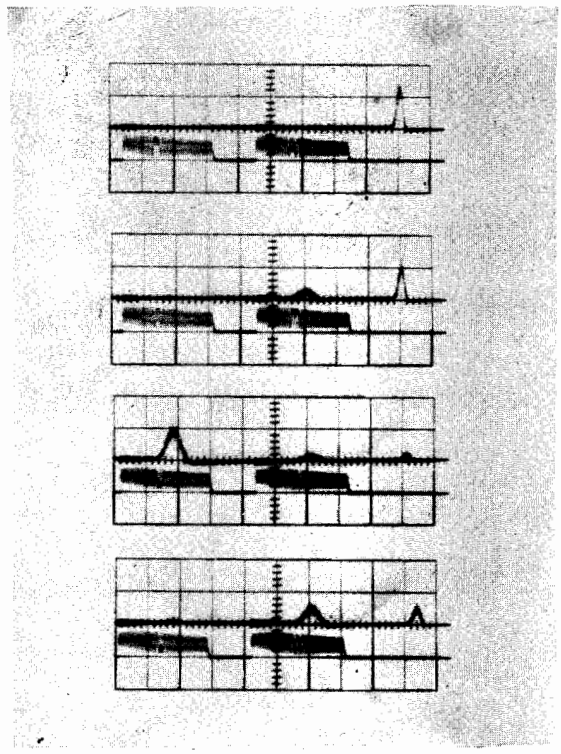

Fig. 16

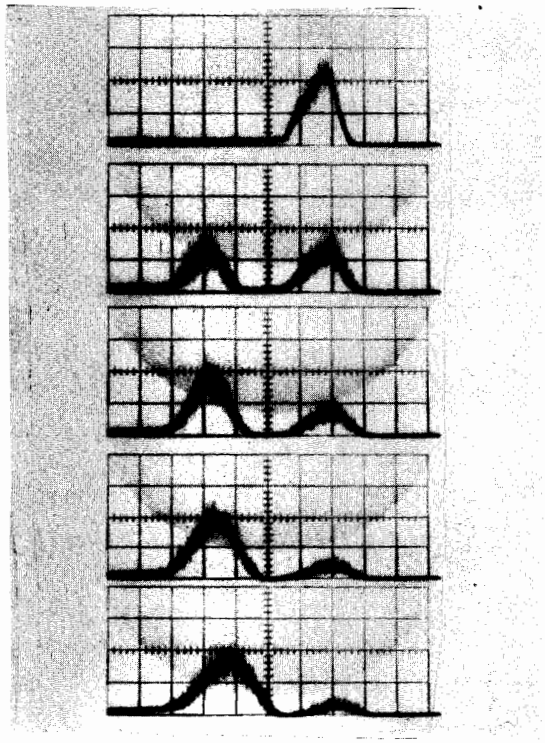

Fig. 17

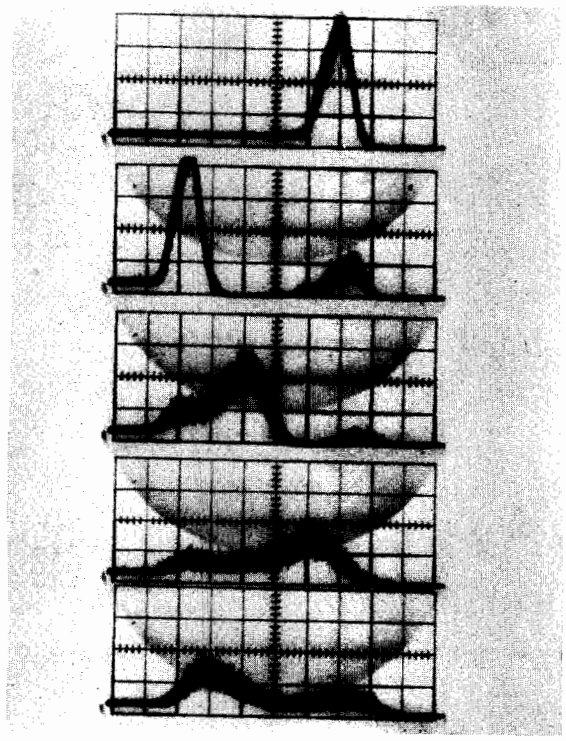

Fig. 18